Quaternary Science Reviews 83 (2014) 157–170

Contents lists available at ScienceDirect

Quaternary Science Reviews

journal homepage: www.elsevier.com/locate/quascirev

Event layers in the Japanese Lake Suigetsu 'SG06' sediment core: description, interpretation and climatic implications

Gordon Schlolaut [a,*], Achim Brauer [a], Michael H. Marshall [b], Takeshi Nakagawa [c], Richard A. Staff [d], Christopher Bronk Ramsey [d], Henry F. Lamb [b], Charlotte L. Bryant [d], Rudolf Naumann [e], Peter Dulski [a], Fiona Brock [d], Yusuke Yokoyama [f,g], Ryuji Tada [f], Tsuyoshi Haraguchi [h], Suigetsu 2006 project members [1]

[a] German Research Centre for Geosciences (GFZ), Section 5.2: Climate Dynamics and Landscape Evolution, Telegrafenberg, 14473 Potsdam, Germany
[b] Institute of Geography and Earth Sciences, Aberystwyth University, SY23 3DB, UK
[c] Department of Geography, University of Newcastle, Newcastle-upon-Tyne NE1 7RU, UK
[d] Oxford Radiocarbon Accelerator Unit (ORAU), Research Laboratory for Archaeology and the History of Art (RLAHA), University of Oxford, Dyson Perrins Building, South Parks Road, Oxford OX1 3QY, UK
[e] German Research Centre for Geosciences (GFZ), Section 4.2: Inorganic and Isotope Geochemistry, Telegrafenberg, 14473 Potsdam, Germany
[f] Department of Earth and Planetary Sciences, Faculty of Science, University of Tokyo, 7-3-1 Hongo, Bunkyo-ku, Tokyo 113-0033, Japan
[g] Ocean Research Institute, University of Tokyo, 1-15-1 Minami-dai, Nakano-ku, Tokyo 164-8639, Japan
[h] Department of Geosciences, Osaka City University, Sugimoto 3-3-138, Sumiyoshi, Osaka 558-8585, Japan

ARTICLE INFO

Article history:
Received 20 June 2013
Received in revised form
20 October 2013
Accepted 24 October 2013
Available online 7 December 2013

Keywords:
Floods
Earthquakes
Microfacies
Microscopy
μXRF
East Asia
Lacustrine
Typhoons
LGM

ABSTRACT

Event layers in lake sediments are indicators of past extreme events, mostly the results of floods or earthquakes. Detailed characterisation of the layers allows the discrimination of the sedimentation processes involved, such as surface runoff, landslides or subaqueous slope failures. These processes can then be interpreted in terms of their triggering mechanisms. Here we present a 40 ka event layer chronology from Lake Suigetsu, Japan. The event layers were characterised using a multi-proxy approach, employing light microscopy and μXRF for microfacies analysis. The vast majority of event layers in Lake Suigetsu was produced by flood events (362 out of 369), allowing the construction of the first long-term, quantitative (with respect to recurrence) and well dated flood chronology from the region. The flood layer frequency shows a high variability over the last 40 ka, and it appears that extreme precipitation events were decoupled from the average long-term precipitation. For instance, the flood layer frequency is highest in the Glacial at around 25 ka BP, at which time Japan was experiencing a generally cold and dry climate. Other cold episodes, such as Heinrich Event 1 or the Late Glacial stadial, show a low flood layer frequency. Both observations together exclude a simple, straightforward relationship with average precipitation and temperature. We argue that, especially during Glacial times, changes in typhoon genesis/typhoon tracks are the most likely control on the flood layer frequency, rather than changes in the monsoon front or snow melts. Spectral analysis of the flood chronology revealed periodic variations on centennial and millennial time scales, with 220 yr, 450 yr and a 2000 yr cyclicity most pronounced. However, the flood layer frequency appears to have not only been influenced by climate changes, but also by changes in erosion rates due to, for instance, earthquakes.

1. Introduction

Earthquakes and precipitation induced floods are two of the major natural hazards faced in Japan, resulting in the loss of human life and the destruction of infrastructure. For a better understanding of how these risks develop over long time scales, palaeo-records are necessary since instrumental records only cover recent history. Both kinds of events can leave an imprint on lake sediments (Arnaud et al., 2002; Beck, 2009; Lauterbach et al., 2012; Gilli et al., 2013), enabling the construction of respective chronologies. Lacustrine flood chronologies especially have received increased attention in recent years, since lake sediments are an ideal archive for such studies (Moreno et al., 2008; Vasskog et al., 2011; Kämpf

* Corresponding author.
E-mail address: gosch@gfz-potsdam.de (G. Schlolaut).
[1] For full details see: www.suigetsu.org.

0277-3791/$ – see front matter © 2013 Elsevier Ltd. All rights reserved.
http://dx.doi.org/10.1016/j.quascirev.2013.10.026

et al., 2012; Gilli et al., 2013) as they are part of the hydrological system and can record flood events as distinct detrital layers (Sturm and Matter, 1978; Mangili et al., 2005; Brauer et al., 2008) over time frames of up to 10^{4-5} years. Furthermore, when these sediments are annually laminated (varved), they also provide excellent chronological control (Cockburn and Lamoreux, 2007; Czymzik et al., 2010; Swierczynski et al., 2012). Such datasets can help us to gain a better understanding of how global climate change forces changes in local to regional flood regimes. However, detailed microfacies analysis of such event layers is necessary in order to distinguish flood events from other major depositional events, such as landslides or subaqueous slope failures (Swierczynski et al., 2012; Wilhelm et al., 2012; Czymzik et al., 2013), which in turn are often the result of earthquakes.

The study of palaeo-floods in Japan has so far mainly relied on the analysis of geomorphological features and sedimentological analysis of fan and terrace deposits, suggesting higher flood magnitudes during the Holocene than during the Last Glacial Maximum (LGM) (Oguchi et al., 2001 and references therein; Grossman, 2001). However, such studies produce more qualitative than quantitative results. Here we present a 40 ka event layer stratigraphy from the Lake Suigetsu sediment. The entire Suigetsu composite sediment sequence is about 73 m, which is estimated to cover the last 150 ka (Nakagawa et al., 2012), with varves occurring between ≈10 and ≈70 ka BP (Staff et al., 2013a). The first (English language) description of the event layers in the Lake Suigetsu sediment was published by Katsuta et al. (2007), who used data from a Scanning X-ray Analytical Microscope (SXAM). They analysed a 6 m long section of the 16 m long "SG3" piston core recovered in 1993 (Kitagawa et al., 1995). Katsuta et al. (2007) used three tephras as age control points and analysed a core interval that they estimated to be between 19,010 and 5670 yr cal BP. They counted 30 event layers (excluding tephras) and identified two types: turbidites and clay layers, which they interpreted to derive from earthquakes (turbidites) and floods (clay layers).

In this study we use the composite "SG06" profile, recovered in 2006 from four bore holes, which is entirely continuous and contains the complete Lake Suigetsu sediment sequence (Nakagawa et al., 2012). The event layers were analysed in the top ≈31 m, which are robustly dated (Bronk Ramsey et al., 2012) and which represent the last ≈40 ka. A multi-proxy approach was applied, utilising thin section microscopy, micro X-ray fluorescence (μXRF) scanning and core photographs.

1.1. Study site

Lake Suigetsu is situated in Fukui prefecture on the west coast of Honshu Island, central Japan. It is part of a tectonic lake system (Mikata Five Lakes) with the active Mikata fault running N–S less than 2 km to the east (Fig. 1). The lake is approximately 2 km in diameter and has a maximum water depth of 34 m (Nakagawa et al., 2005).

In AD 1664 a canal was built connecting Lake Suigetsu with Lake Kugushi, which resulted in the inflow of salt water (Masuzawa and Kitano, 1982; Kondo et al., 2009). The reason for the channel construction was an earthquake in AD 1662, which displaced the outlet of the lake system, resulting in a lake level rise and the inundation of rice fields and villages around the lakes (Kawakami et al., 1996). The channel was built as drainage for the lake system.

The lake system is fed with fresh water by the Hasu River, which flows into Lake Mikata, which in turn is connected to Lake Suigetsu by a shallow (<4 m deep) sill. In this setting Lake Mikata acts as a natural filter for coarse detrital material from the Hasu River catchment (Nakagawa et al., 2005), resulting in sedimentation of predominantly autochthonous and authigenic material in Lake Suigetsu (Schlolaut et al., 2012).

The geology around the lake is dominated by a large granite pluton to the E and SE. To the S mudstone dominates, but also sandstone, chert, limestone, basalt and dolerite occur. At the NE coast of the lake sandstone occurs, while at the N and W coast

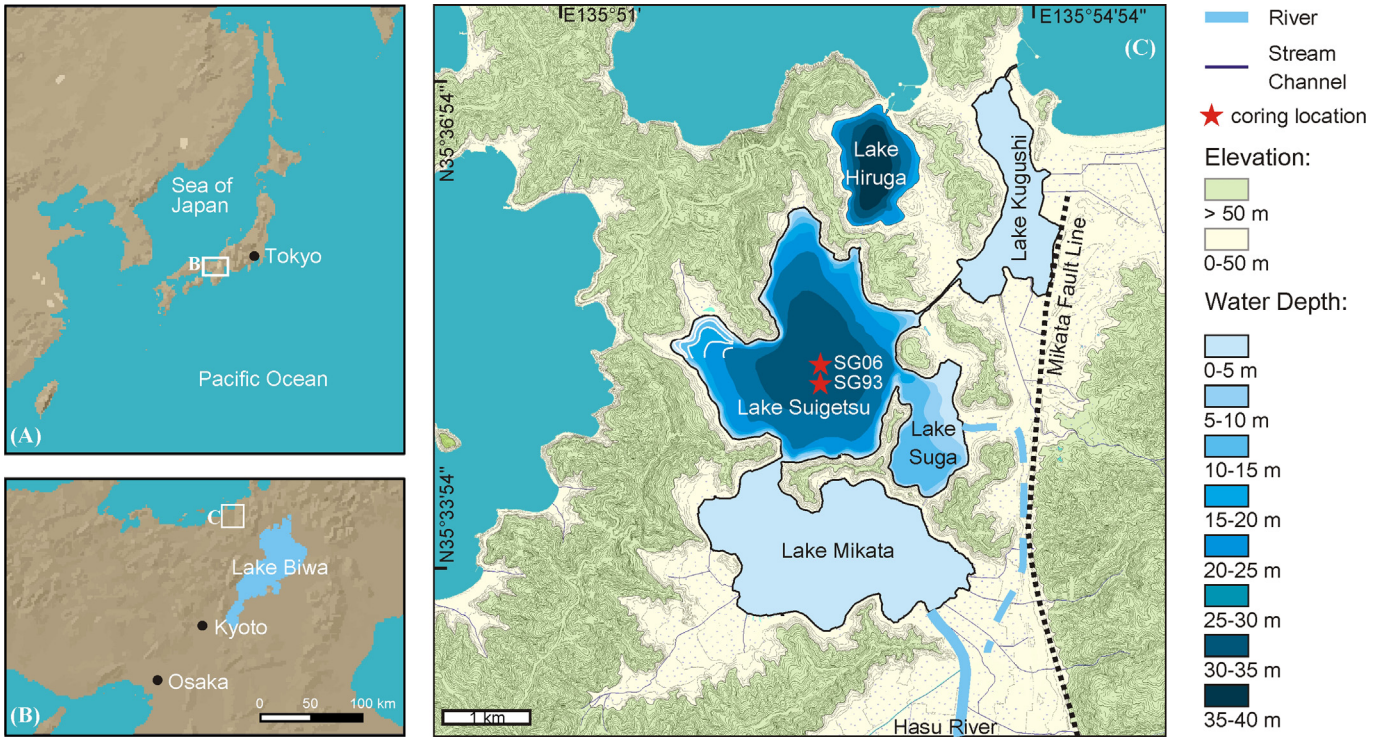

Fig. 1. Location of Lake Suigetsu (modified after Nakagawa et al. (2012) and topographic map of the Geospatial Information Authority of Japan). The dashed river line shows the hypothesised palaeo river bed of the Hasu River. White bathymetric lines in the western cove of Lake Suigetsu are manually interpolated.

basalt, dolerite and chert are dominant (*geological map of the Geological Survey of Japan, Agency of Industrial Science and Technology, 2002*).

The climate at Lake Suigetsu is influenced by the East Asian Monsoon (EAM) system, with the site being north of the monsoon front in winter and south of it in summer (Nakagawa et al., 2006). The summer rainy season lasts from June to July and can lead to catastrophic floods (Fukutome et al., 2003). Precipitation is also high during winter when dry and cold monsoon winds from the Asian continent pick up heat and moisture from the Sea of Japan, leading to increased snowfall along the central western shore of Japan (Takano et al., 2008). The heat is provided by the Tsushima current, which is a branch of the warm Kuroshio current entering the Sea of Japan. Furthermore, Japan is frequently affected by typhoons, for which the peak season is August to September.

2. Materials and methods

Core photographs, thin sections and thin section scans were used to identify event layers, and μXRF data to additionally characterise these geochemically. Identification was based on the layers' colour and internal structure. They were considered event layers when they were distinct in both the core photograph and the thin section, and when they were macroscopically identifiable, i.e. when they were clearly distinguishable with the naked eye in the core photograph and the thin section scan. This translates into a minimum thickness of about 1–2 mm. Tephras were not considered in this study (results from tephra analysis can be found in Smith et al. (2013)). For the upper 1288 cm composite depth (cd – model version 24 Aug 2009 (Nakagawa et al., 2012)) of the profile no thin sections and no μXRF data were available, as both methods were primarily intended for varve counting and lamination is generally poor above 1288 cm cd (≈10,200 yr BP). Hence, event layer identification was based solely on core photographs in the upper part. As a result, the reliability of the dataset is reduced there. However, based on experience from the lower core section, impairment of the identification and classification of layers is expected to be minor. Therefore, the reliability of the dataset in the upper core section is considered acceptable. The analysis was carried out down to 3167.7 cm cd, which marks the current lower end of the varve count-based age model (Bronk Ramsey et al., 2012).

The number of event layers in this study is not identical with that in the event layer list used for calculating the event free depth, which was used in previous SG06 publications for interpolating age models (Bronk Ramsey et al., 2012; Schlolaut et al., 2012). In the latter only event layers with a thickness of ≥4 mm have been included whereas this study comprises also thinner event layers.

The nomenclature used here is EL for event layer followed by the composite depth of the base of the layer (in cm), e.g. EL-3165.4.

2.1. Core photographs

Digital core photographs were taken directly after core opening in the field, before colour changes due to oxidation could occur. The pictures were taken under natural daylight and include a scale and a colour chart (Nakagawa et al., 2012).

2.2. Thin section microscopy

For thin section preparation the sediment in the LL-channels (Nakagawa et al., 2012) was cut into 10 cm long segments and freeze-dried. Afterwards, the samples were impregnated with synthetic resin under vacuum. The blocks produced were glued to glass slides with the same resin and then cut, ground and polished down until a ≈20 μm thin slice remained on the glass slide (Brauer and Casanova, 2001). A petrographic microscope with magnification from 25× to 400× was used for analysis. Additionally, thin sections were scanned in polarised light with a 1200 dpi resolution. These thin section scans provide an ideal tool to link core photographs and thin sections, using standard image processing software.

2.3. μXRF analysis of core material

For μXRF analysis continuous measurements were made from 1288 cm cd to the base of the core with an ITRAX core scanner on the sediment in the LL-channels. The distinctive feature of the ITRAX core scanner is the generation of a flat X-ray beam, measuring a rectangular window rather than a single spot. In this way, grain to grain variances are averaged across the horizontal core axis. For the Suigetsu sediment a 20 × 0.1 mm rectangular beam was used, with a step-size of 60 μm, a count time of 4 s, a voltage of 30 kV, a current of 30 mA and a Mo X-ray tube. A more detailed description of the settings used is given by Marshall et al. (2012).

2.4. XRF analysis of catchment samples

In a pilot study 23 catchment samples from around the lake and the proximal watershed of the Hasu River were analysed. Samples included soils, rocks, stream and rivulet sediments. The samples were freeze-dried, powdered and sieved to <62 μm particle size. Samples were prepared as fused disks of Li tetraborate–metaborate (FLUXANA FX-X65, sample-to-flux ratio 1:6). A Panalytical Axios Advanced wavelength-dispersive spectrometer and matrix correction programs were used to calculate concentrations. H_2O^+ and CO_2 were determined using a Vario EL III (Elementar Analysensysteme GmbH, Hanau/Germany) by means of high-temperature catalytic combustion.

2.5. Age model

The age model of the SG06 core (Staff et al., 2013a) after 11.2 ka BP uses high resolution ^{14}C data from SG06 modelled on to the IntCal09 calibration curve (Reimer et al., 2009; Staff et al., 2011), while the older part is based on a varve count chronology, which has been created using a dual-method counting approach utilising thin section microscopy and μXRF measurements (Marshall et al., 2012; Schlolaut et al., 2012). This varve chronology was then constrained by the Bahamas speleothem GB89-25-3 (Hoffmann et al., 2010) and the Hulu Cave speleothem H82 (Southon et al., 2012) U–Th chronologies, using the low frequency ^{14}C signal from Lake Suigetsu to link with the ^{14}C data from the speleothems (Bronk Ramsey et al., 2012). The resulting chronology is given in "$SG06_{2012}$ yr BP".

3. Results

3.1. Sediment characterisation and major facies changes

The Lake Suigetsu sediment consists of organic material, diatoms, siderite and detrital mineral grains. All of these components occur diffusely (i.e. form the sediment matrix), but also as distinct (seasonal) layers (Schlolaut et al., 2012). From the top down to 3095.9 cm cd the analysed core section is usually dominated by the autochthonous components, while below it contains a higher proportion of detrital mineral grains. The boundary between the two facies is marked by the top of event layer EL-3107 (event layer type II, see Section 3.2.2). The facies change is evident in the μXRF signal too, showing a clear drop in Ti and Ca in the upper core

section, as well as a weak drop in K (Fig. 2) and it is also visible in the core photograph, where the colour changes from a light grey in the lower part to a dark grey in the upper.

3.2. Event layer types

A total of three different event layer types were distinguished by microfacies analysis, labelled type I, II and III. The total number of event layers is 369, from which 362 are type I, 2 are type II and 5 are type III.

For characterising the clastic event layers in the SG06 profile by μXRF, the elements Ti, K, Ca and Si are most suitable. Ti is a well established tracer element for terrigeneous input (e.g. Yarincik and Murray, 2000), K indicates the presence of clays and/or K-feldspar and Ca may derive from detrital carbonates or plagioclase. The Si signature of the event layers is not as distinct as that of the other elements – the reason being that the sediment is rich in diatoms and hence generally rich in Si. Therefore, the Si signal in the event layer is only slightly elevated compared to the surrounding sediment. However, it is the most suitable element to distinguish the I-B sub-layer in type I event layers (see below). Additionally, Fe and Mn were considered as these two elements play a major role in the hydrology and sedimentation of the lake (Katsuta et al., 2006, 2007; Marshall et al., 2012).

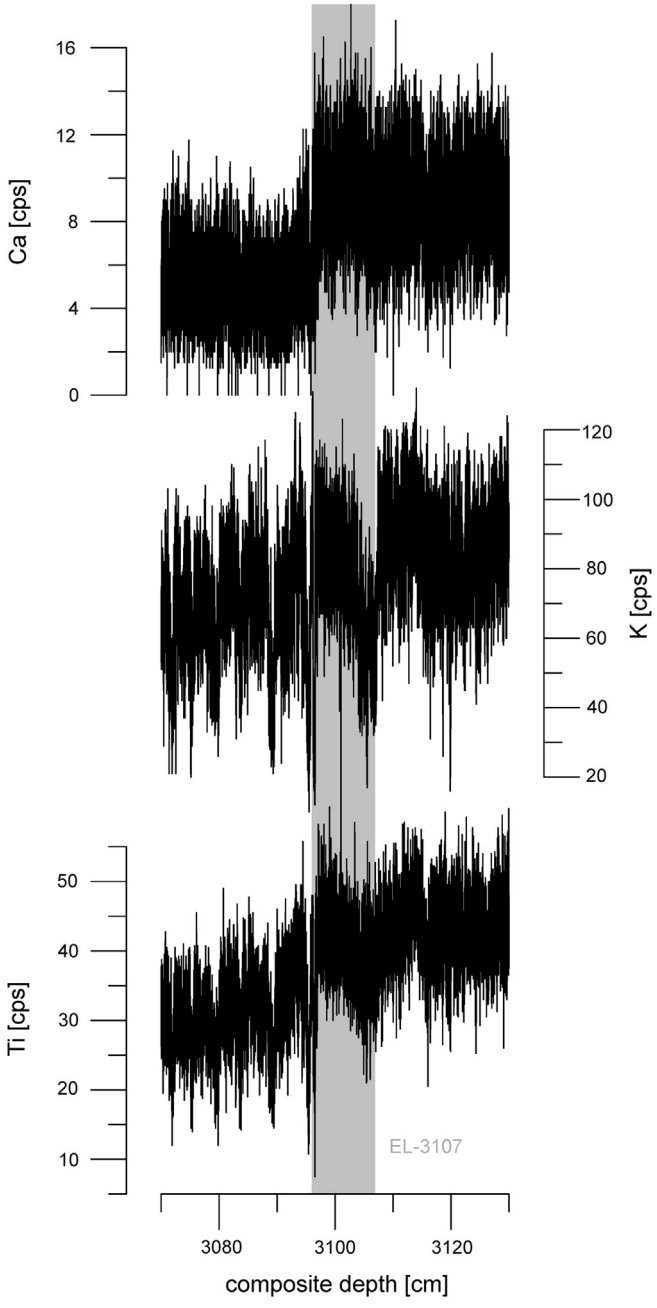

Fig. 2. Changes in Ti (lower), K (middle) and Ca (upper) at the facies boundary at the top of event layer EL-3107 (marked in grey).

3.2.1. Event layer type I

The structure of an ideal type I event layers comprises four main sub-layers (Fig. 3). The basal sub-layer (I-A) consists primarily of quartz and feldspar intermingled with autochthonous components, mainly diatoms and amorphous organic material, but also leaf and wood fragments. The detrital minerals in this sub-layer reach grain sizes of coarse silt and show no significant grading.

The following sub-layer, I-B, consists of quartz and feldspar and, towards the top, also clay. The sub-layer contains only very minor amounts of autochthonous material. No plant fragments are found in this or the following sub-layers. The sub-layer shows distinct normal grading, starting with medium to fine silt, decreasing to clay sized minerals.

Above follows a sub-layer (I-C) of homogenous, clay sized detrital material, with an increased proportion of clay minerals. Otherwise, mineral grains are usually too small to reliably identify the mineral type by light microscopy. Autochthonous material is usually absent.

The top sub-layer (I-D) is a mixture of detrital material and the sediment matrix. It is highly variable in the proportion of these two components, the grain size of the detrital minerals, as well as in its thickness. Often the upper boundary of this sub-layer is indistinct and it gradually fades into the sediment matrix.

In the μXRF signal (Fig. 3) the I-A sub-layer is characterised by increased Ti, K and Ca values. At the base of I-B, Ti and K increase further and then decrease towards the top of the event layer. Ca starts to decrease from the base of I-B. Si shows a distinct peak in the I-B layer. The boundary between I-C and I-D cannot be identified reliably in the μXRF signal. Fe and Mn show no variability within this event layer type and thus are not depicted in Fig. 3.

In the core photographs (Fig. 3) sub-layer I-A can be distinguished by its greyish colour, while the three upper sub-layers show no clear boundaries between themselves and appear as one 'clay cap' of light grey colour.

In most cases I-A sub-layers are absent and only the characteristic clay cap is found commonly comprising sub-layers I-B, I-C and I-D. From all 279 type I event layers in the sediment interval in which microfacies analyses could be applied (from 1288 to 3167.7 cm cd) only in 12 layers a I-A sub-layer has been identified. A high lateral thickness variability of the I-A sub-layers is shown in Fig. 3, where the same event layer was identified in an SG06 and an 'SG93' thin section. SG93 was a predecessor project of SG06 (Kitagawa and van der Plicht, 2000; Staff et al., 2013b) but thin sections from SG93 were only available for a part of the Last Glacial–Interglacial Transition (LGIT, also Last Termination or Late Glacial) and contained only one event layer with a clear I-A sub-layer. In this event layer (EL-1431.2) the I-A sub-layer has a thickness of ≈20 mm in SG06, but only ≈1 mm in SG93.

Type I event layers occur repeatedly above siderite layers and layers of amorphous organic material (LAO layers). Both layers have been identified as seasonal layers and relate to autumn and summer respectively (Schlolaut et al., 2012), placing the type I event layers into autumn. That a seasonal layer does not occur below every type I event layer is simply due to the fact that not every year

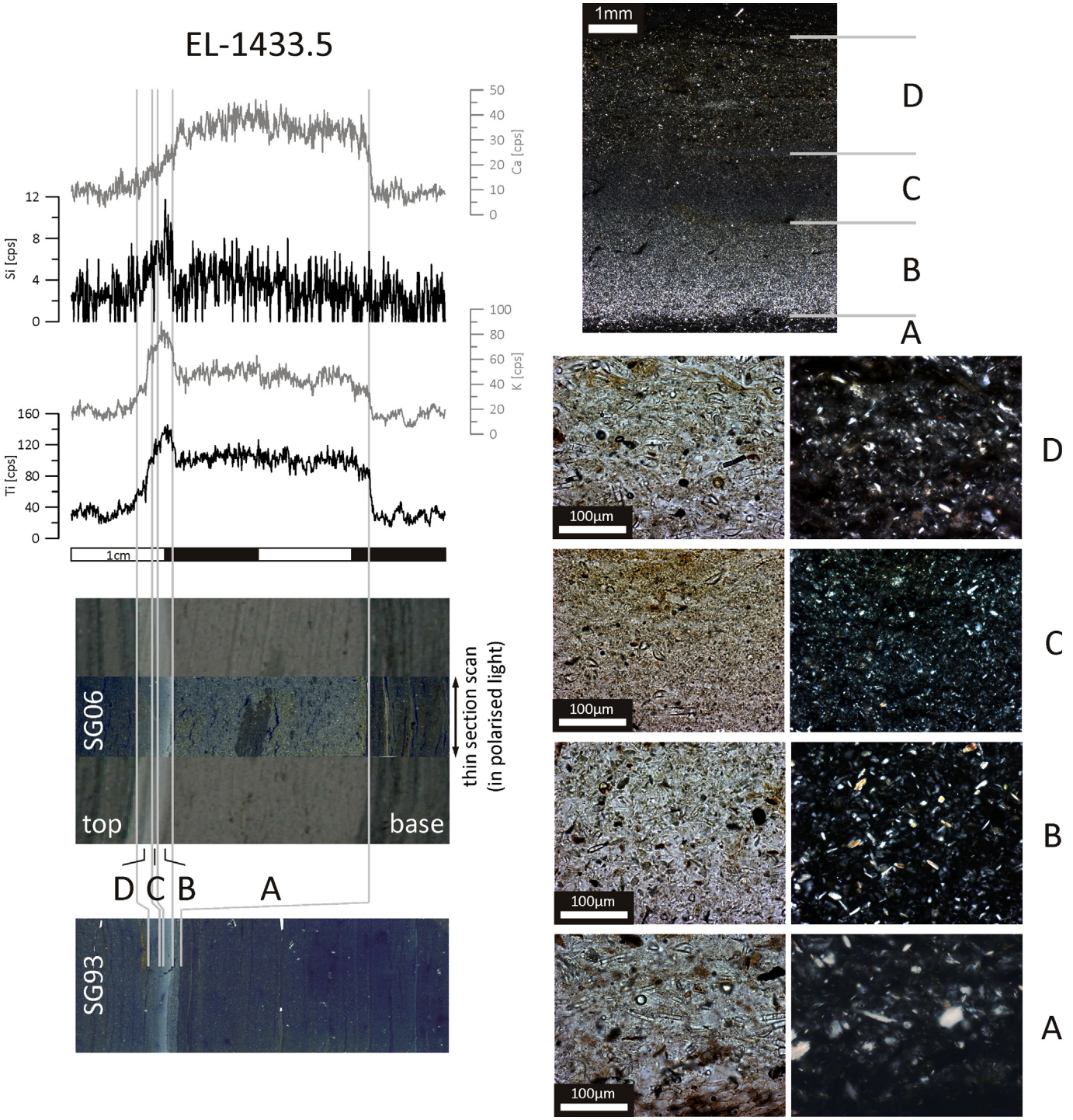

Fig. 3. Microfacies of event layer type I: left panel shows µXRF scans aligned to the core photo, overlain by a thin section scan in polarised light and below the thin section scan from SG93 containing the same event layer. In the upper right a microscope photo shows the detailed structure of the 'clay cap'. The lower right panel shows microscope photos of the different sub-layers in plain (left) and polarised (right) light.

seasonal layers formed. The relationship between the event and seasonal layers is best observed in the LGIT, where the frequency of the seasonal layers is much higher than in the Glacial. In the Glacial a reliable season placement is not possible.

3.2.2. Event layer type II

Only two layers of type II occur in the analysed interval (EL-2244.2, EL-3107). They appear to be rather similar to type I layers in the core photos, consisting of a coarse base and a clay top, but micro-facies and µXRF analyses show significant differences (Fig. 4). Most notably, type II event layers consist of 5 rather than 4 sub-layers and contain much larger plant fragments and siderite. Furthermore, Ti and K values tend to decrease rather than increase. The coarse base of type II event layers consists of 4 sub-layers, whereas with type I layers it is a single sub-layer (I-A). The bottom sub-layer of type II event layers (II-A) is similar to the I-A sub-

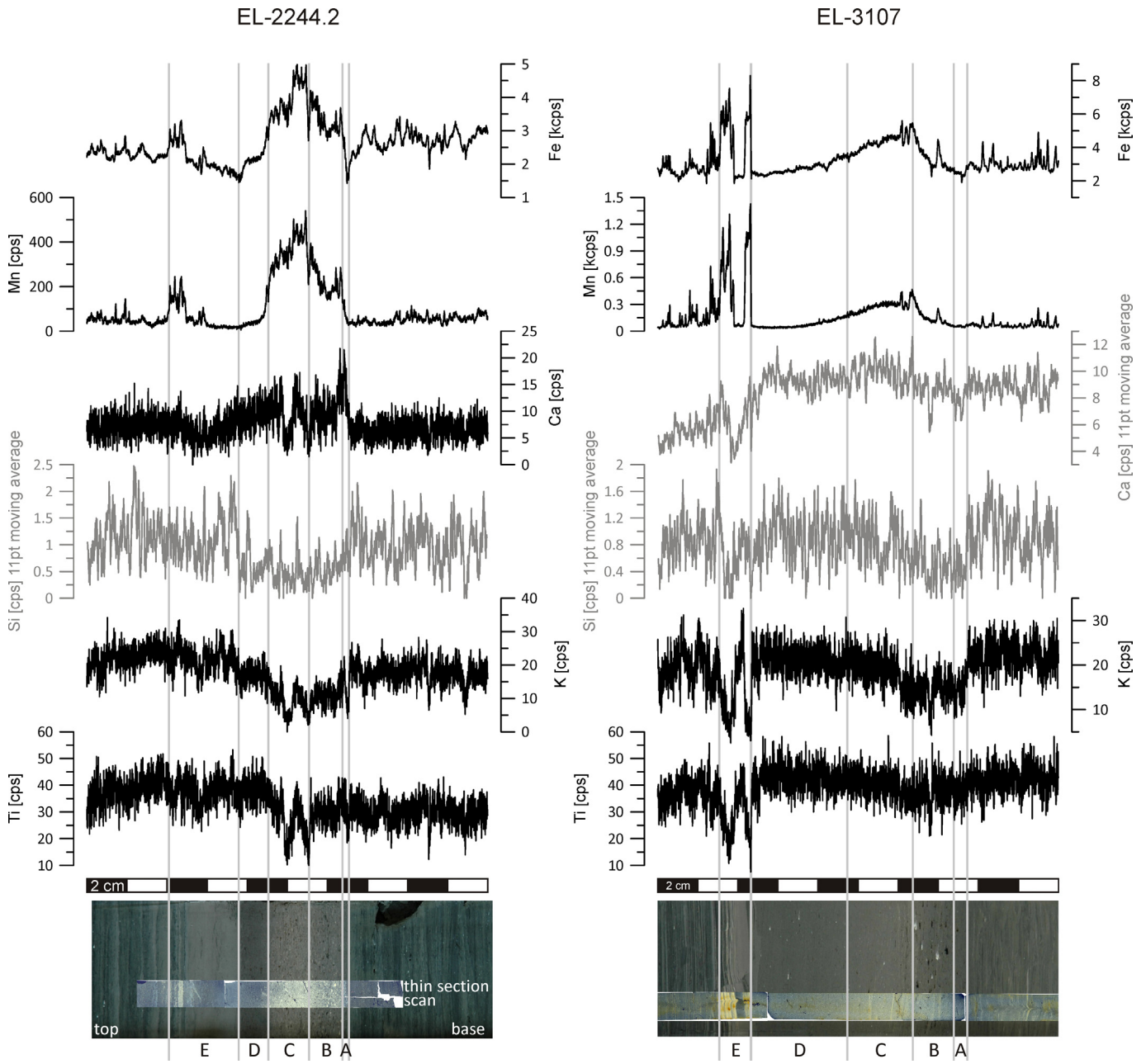

Fig. 4. Microfacies of event layer type II: μXRF scans aligned with core photos, overlain by thin section scans in polarised light. The left panel shows EL-2244.2, the right panel EL-3107. Grey μXRF curves show the 11 pt moving average.

layer, but reaches larger grain sizes (coarse silt to fine sand). In the II-B sub-layer siderite occurs and plant fragments are much larger than in type I event layers (up to 1 mm). In the case of EL-2244.2 the sub-layer is also enriched in amorphous organic material, which is a component of the sediment matrix. In the following two sub-layers (II-C, II-D) grain sizes, size and number of plant fragments and siderite concentrations, which reached maximum values at the base of II-C, decrease. Furthermore, the amorphous organic material increases in II-C in EL-2244.2. The top sub-layer (II-E) is characterised by a clearly graded silt/clay layer, intercalated with siderite layers, which are rather massive in EL-3107.

In the μXRF data (Fig. 4) the layer type is characterised by high Fe and Mn values, increasing from the base of the II-B sub-layer to the lower part of II-C, then decreasing again to the normal background values in II-D. In the II-E sub-layer clear peaks occur at the positions of the siderite layers. The other elements (Ti, K, Ca, Si) do not give as clear a type-specific signal, with the signal to noise ratio being clearly lower than in type I event layers. The four elements differ slightly between the two type II event layers. However, K shows a clear tendency to, and Ti and Si a slight tendency to lower values in II-B and II-C, while Ca values tend to be elevated from II-A to II-D.

3.2.3. *Event layer type III*

The 5 event layers of type III are matrix supported layers, characterised by a distinctly homogenous structure and a high proportion of material from the sediment matrix (Fig. 5). For this reason event layers of type III are much more difficult to distinguish in the core photographs than the other two types. Hence, identification in

the upper core interval, above 1288 cm cd (where identification is based solely on core photographs), is less reliable for this layer type. Only 1 of the 5 identified layers lies in the upper part (EL-91). From the 4 event layers that can be characterised by microscopy 3 differ from the surrounding sediment matrix by containing an increased number of larger mineral grains (about 3–7 times larger, reaching fine to medium sand). At the top of these 3 layers a cap of large lenses of aggregated siderite occurs. The 4th event layer (EL-1731.8) exhibits only a homogenous structure. The type III layers show no common signature in the μXRF signal. Two of them are rather similar to the sediment matrix in the μXRF signal and thus difficult to distinguish (EL-1731.8, EL-1979.2), whereas EL-1632.6 shows distinctly increased values of Ti, K and Ca, and EL-2464.5 is characterized by a weak increase in Ca and K and a distinct increase in Fe and Mn. The siderite caps are further enriched in Mn.

3.3. Event layer type I frequency

The type I event layer frequency shows a high variability over the past ≈40 ka, reaching from 0 up to 22 event layers per 1000 years (Fig. 6). Based on the mean frequency the curve can be divided into 5 zones (FLZ – flood layer zone, for event layer interpretation see next section).

The lowermost zone, FLZ5, reaches to about 35,750 $SG06_{2012}$ yr BP (rounded to half a century) and is characterised by about 13 flood layers per 1000 yr.

The following zone, FLZ4, shows about 3 flood layers per 1000 yr, but reaches a maximum of 8 layers per 1000 yr in a well defined peak at around 33,900 $SG06_{2012}$ yr BP. The boundary between this and the next zone coincides with the AT tephra (30,009 ± 189 $SG06_{2012}$ yr BP (Smith et al., 2013)).

Zone FLZ3 has the highest mean value of 13 layers per 1000 yr and also reaches the highest maximum value of 22 layers per 1000 yr. It also exhibits a strong cyclicity with $T \approx 2000$ yr. Based on the per 100 yr plot, FLZ3 can be divided into two sub-zones: FLZ3a (upper) and FLZ3b (lower). The lower subzone shows a higher frequency of flood layers (3–4 per 100 yr) than the upper zone (2 per 100 yr). The boundary between the two sub-zones lies at about 23,450 $SG06_{2012}$ yr BP and the upper boundary of FLZ3 at 18,500 $SG06_{2012}$ yr BP. The timing of FLZ3 is approximately contemporaneous with the global sea level minimum of the Last Glacial (30–19 ka BP, Lambeck et al., 2002).

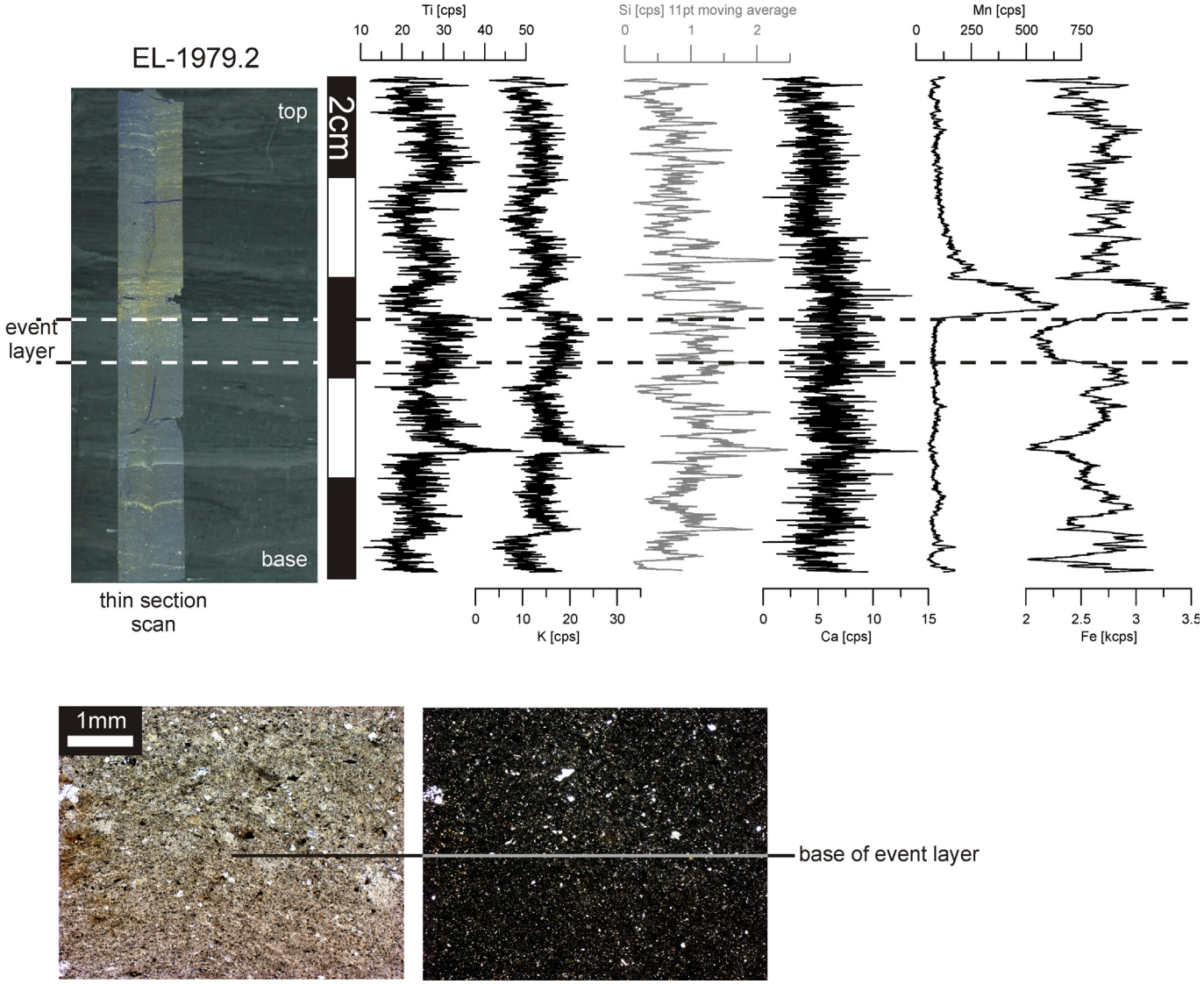

Fig. 5. Microfacies of event layer type III: top panel shows μXRF scans aligned to the core photo, overlain by a thin section scan in polarised light (note that the μXRF signature is not to be considered layer type specific, see text Section 3.2.3 for details); bottom panel shows microscope photos of the base of the layer in plain (left) and polarised (right) light.

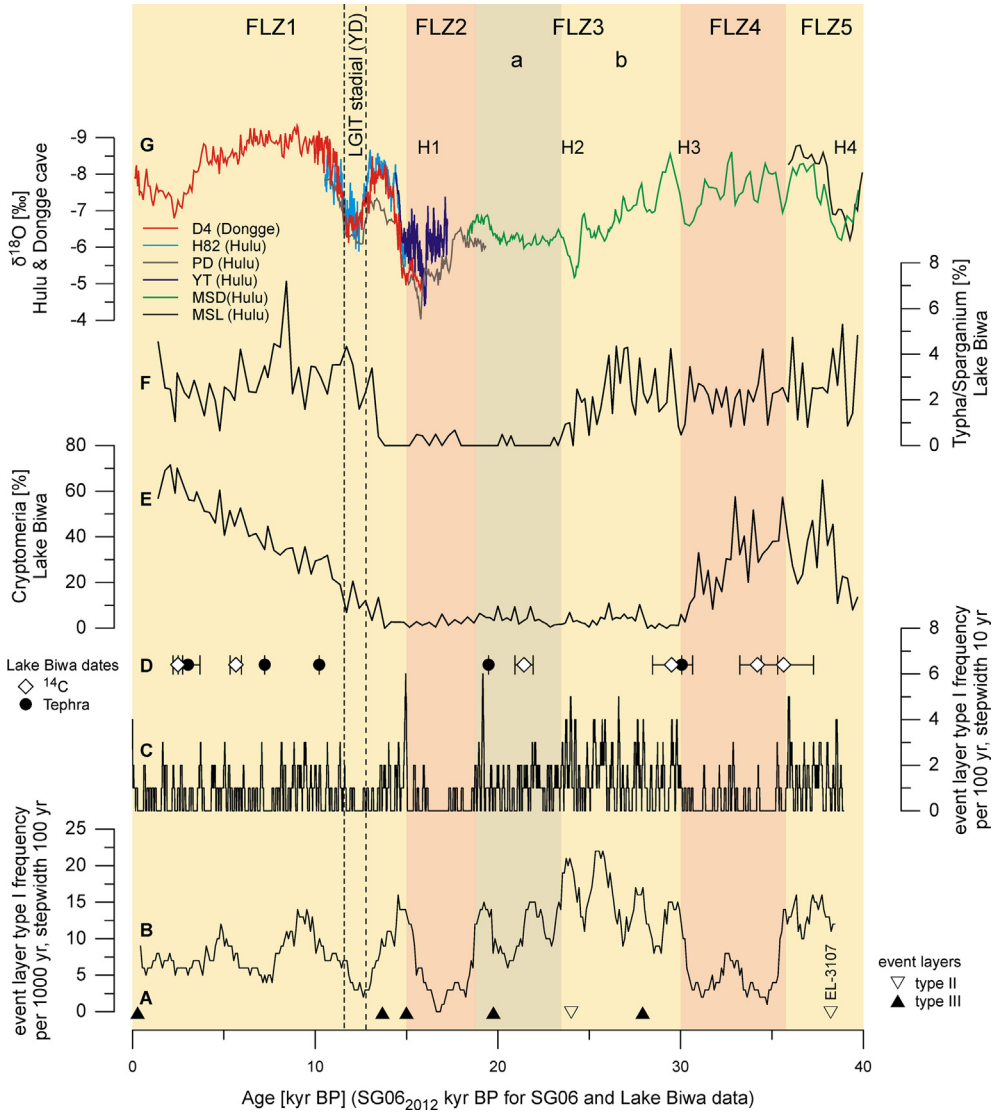

Fig. 6. A: position of type II and III event layers; B: SG06 flood layer frequency per 1000 yr; C: SG06 flood layer frequency per 100 yr; D: position and type of Lake Biwa dates (Hayashi et al., 2010); E & F: pollen curves from Lake Biwa (Hayashi et al., 2010) (For better comparison of the SG06 and Lake Biwa data the age model of Hayashi et al. (2010) was transferred to the SG06$_{2012}$ yr BP age scale, using tephras as isochrons and modelling the ^{14}C dates on to the SG06$_{2012}$ yr BP age scale. A discrepancy can be observed at the onset of the LGIT, which is considerably younger in the Lake Biwa data. This we relate to the fact that it falls into a 10 ka long interval, which is only constrained by two tephras, the U-Oki (10,217 ± 40 SG06$_{2012}$ yr BP; Staff et al., 2013a; Smith et al., 2013) and the Sakata tephra (19,487 ± 112 SG06$_{2012}$ yr BP; Smith et al., 2013). Some major climate changes fall into this time frame, so that the assumption of a near linear mean sedimentation rate between these two points in Lake Biwa might be invalid. Nevertheless, the pollen data can still be used to characterise the general climate conditions in central Japan over the last 40 ka.); G: U–Th dated Chinese speleothem records of δ^{18}O from Hulu and Dongge cave (Wang et al., 2001; Yuan et al., 2004); Heinrich Events are labelled H1 to H4. Flood layer zones (FLZ) are labelled at the top.

The next zone, FLZ2, shows the lowest values from all zones, with between 0 and 4 layers per 1000 yr. It ends at about 15,000 SG06$_{2012}$ yr BP, which coincides with the onset of the LGIT. Therefore, FLZ2 is approximately synchronous with Heinrich Event 1 (H1, 19–15 ka BP, Stanford et al., 2011).

The top-most zone, FLZ1, comprises the Holocene and the LGIT and reaches to the top of the core. The flood layer frequency is generally as low as 6 per 1000 yr, but shows three distinct peaks at ≈15,000 SG06$_{2012}$ yr BP, ≈9500 SG06$_{2012}$ yr BP and ≈5000 SG06$_{2012}$ yr BP, where values reach between 12 and 18 layers per 1000 yr. A distinct minimum occurs during the LGIT stadial (climatic equivalent of the European Younger Dryas pollen zone (Jessen, 1935; Mangerud et al., 1974)).

Frequency analysis of the per 100 yr data (Fig. 7) using REDFIT software (Schulz and Stattegger, 1997; Schulz and Mudelsee, 2002) suggests cycles at $T \approx 220$ yr, $T \approx 450$ yr and $T \approx 5000$ yr, while the per 1000 yr data suggest $T \approx 2000$ yr and $T \approx 5000$ yr. Wavelet analysis (Torrence and Compo, 1998) of the per 100 yr data (Fig. 7e) also clearly shows bands around $T \approx 2000$ yr and $T \approx 5000$ yr, while the bands at smaller periodicities are less well defined.

3.4. XRF analysis of catchment samples

A central finding from the analysis of the catchment samples (Fig. 8) is a strong anti-correlation between Ti and K ($R = -0.72$). K is enriched (defined as greater than the mean value of all samples) in samples that are influenced by the granite pluton to the East, while the highest Ti values are found in the distal watershed of the Hasu River in the South and at the Northeast coast of the lake. The data also show that Ca is generally low. The highest values are found in the tributary streams of the Hasu River, especially in the southernmost samples. Only 2 out of 10 samples in which Ca values

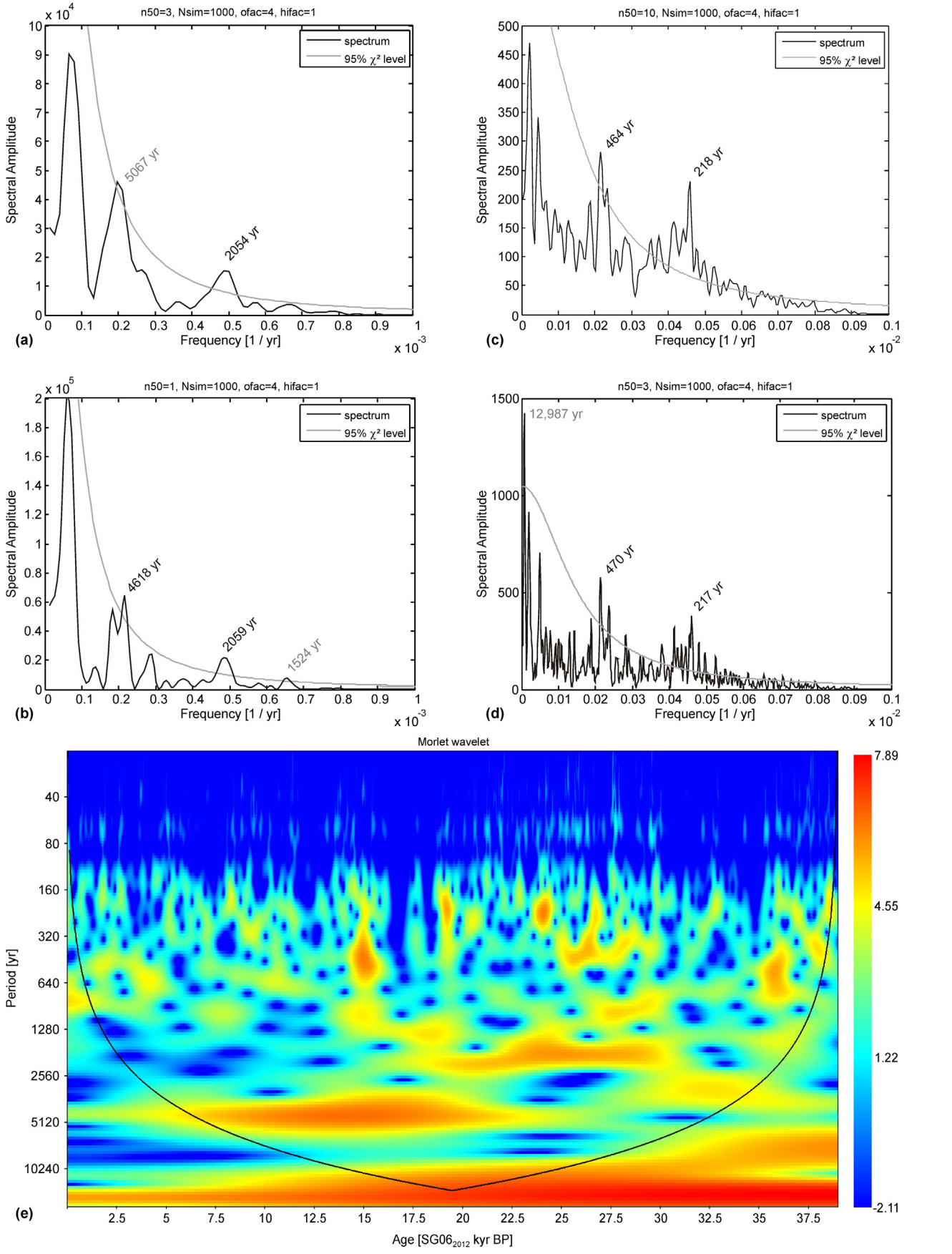

Fig. 7. Periodograms from flood layer frequency data per 1000 yr with: (a) n50 = 3 and (b) n50 = 1, and from data per 100 yr with (c) n50 = 10 and (d) n50 = 3; n50 gives the number of segments with 50% overlap, ofac is the oversampling factor, hifac is the factor for highest frequency (see Schulz and Stattegger (1997) for details). Cycles marked in light grey are considered problematic as they are very close to the 95% χ^2 level or too large considering the length of the dataset. (e) Wavelet analysis of the per 100 yr data using a Morlet wavelet.

were greater than the mean were found directly at the lake, both from the Northeastern shore.

4. Discussion

4.1. Interpretation of event layers

Event layers of type I and II show some similarities, as they consist of coarse detrital material mixed with plant fragments and autochthonous material, overlain by graded silt/clay (Figs. 3 and 4). Such sequences are typical of erosional hyperpycnal turbidity flows (Mulder and Alexander, 2001; Mangili et al., 2005; Gilli et al., 2013) and may be the result of flood events or landslides (possibly triggered by earthquakes) (Swierczynski et al., 2012; Gilli et al., 2013).

Considering the seasonality (occurrence often above siderite or LAO layers in the LGIT) and the high frequency of type I event layers, it is likely that type I layers are related to flood events. In contrast, type II event layers are likely to be related to landslides. This is, for instance, indicated by the μXRF data. In type I event layers Ti and K are enriched and correlate well (e.g. $R_{EL-1298.3} = 0.858$, $R_{EL-1442.5} = 0.857$), which means that the source area of the material includes the Ti rich (in the South) and the K rich (East) regions. In contrast, K and Ti correlate less well in type II events. The layers are clearly depleted in K and only slightly depleted in Ti ($R_{EL2244.2} = 0.687$, $R_{EL-3107} = 0.581$), meaning that the source area was local, excluding stream and soil material influenced by the pluton, possibly deriving directly from the Northeastern shore area.

This interpretation is further supported by the microfacies data, which show larger plant fragments and larger mineral grains in type II layers, as well as a more erosive character (higher proportion of material from the sediment matrix in EL-2244.2), which suggests a higher energy flow, which could be the result of a shorter distance between source and lake (Swierczynski et al., 2012). Whether or not EL-3107 is enriched in material from the sediment matrix is uncertain because the layer occurs within the detrital-rich facies so

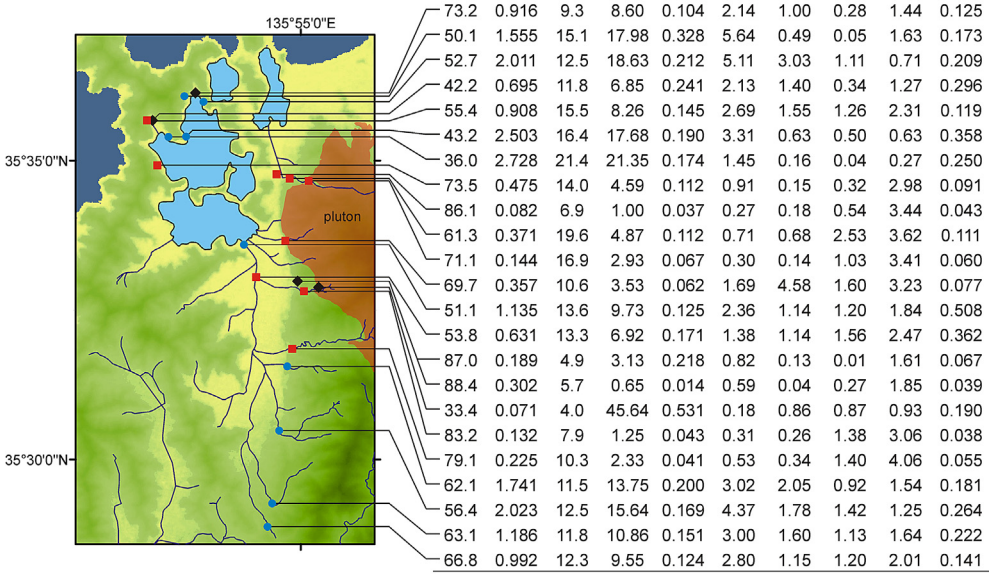

SiO_2	TiO_2	Al_2O_3	Fe_2O_3	MnO	MgO	CaO	Na_2O	K_2O	P_2O_5
73.2	0.916	9.3	8.60	0.104	2.14	1.00	0.28	1.44	0.125
50.1	1.555	15.1	17.98	0.328	5.64	0.49	0.05	1.63	0.173
52.7	2.011	12.5	18.63	0.212	5.11	3.03	1.11	0.71	0.209
42.2	0.695	11.8	6.85	0.241	2.13	1.40	0.34	1.27	0.296
55.4	0.908	15.5	8.26	0.145	2.69	1.55	1.26	2.31	0.119
43.2	2.503	16.4	17.68	0.190	3.31	0.63	0.50	0.63	0.358
36.0	2.728	21.4	21.35	0.174	1.45	0.16	0.04	0.27	0.250
73.5	0.475	14.0	4.59	0.112	0.91	0.15	0.32	2.98	0.091
86.1	0.082	6.9	1.00	0.037	0.27	0.18	0.54	3.44	0.043
61.3	0.371	19.6	4.87	0.112	0.71	0.68	2.53	3.62	0.111
71.1	0.144	16.9	2.93	0.067	0.30	0.14	1.03	3.41	0.060
69.7	0.357	10.6	3.53	0.062	1.69	4.58	1.60	3.23	0.077
51.1	1.135	13.6	9.73	0.125	2.36	1.14	1.20	1.84	0.508
53.8	0.631	13.3	6.92	0.171	1.38	1.14	1.56	2.47	0.362
87.0	0.189	4.9	3.13	0.218	0.82	0.13	0.01	1.61	0.067
88.4	0.302	5.7	0.65	0.014	0.59	0.04	0.27	1.85	0.039
33.4	0.071	4.0	45.64	0.531	0.18	0.86	0.87	0.93	0.190
83.2	0.132	7.9	1.25	0.043	0.31	0.26	1.38	3.06	0.038
79.1	0.225	10.3	2.33	0.041	0.53	0.34	1.40	4.06	0.055
62.1	1.741	11.5	13.75	0.200	3.02	2.05	0.92	1.54	0.181
56.4	2.023	12.5	15.64	0.169	4.37	1.78	1.42	1.25	0.264
63.1	1.186	11.8	10.86	0.151	3.00	1.60	1.13	1.64	0.222
66.8	0.992	12.3	9.55	0.124	2.80	1.15	1.20	2.01	0.141

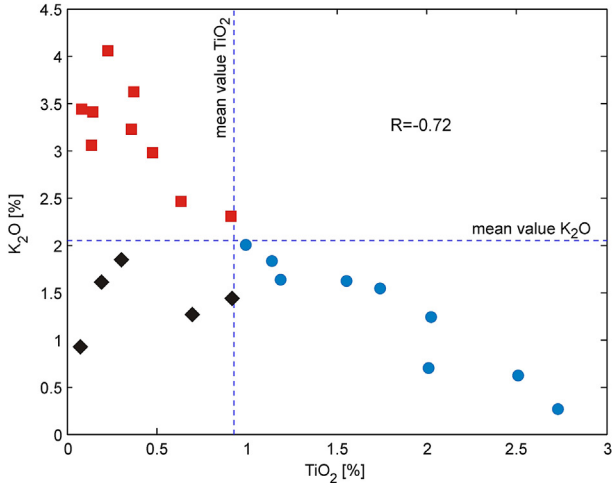

Fig. 8. Locations of catchment samples and XRF composition values [%]; scatter plot shows the anticorrelation between Ti and K; red squares mark samples with K values higher than the mean K value and Ti lower than the mean Ti value, blue circles vice versa (K lower than mean, Ti higher than mean) and black diamonds mark samples in which both elements are below their mean value. (For interpretation of the references to colour in this figure legend, the reader is referred to the web version of this article.)

that redeposited material is also enriched in detrital matter, which is not distinguishable from the detrital material of the event layer itself. Siderite formation within type II event layers might have been favoured by erosion of iron-rich soils as part of a landslide.

Event layers of type III are likely to be the result of subaqueous slope failures. The high proportion of autochthonous components argues against an origin from outside the lake and the large detrital grains (3–7 times larger than in the surrounding sediment) indicate a source closer to the lake shore (i.e. away from the lake centre). The fact that the event layers have no common μXRF signature indicates that they originate from different parts of the lake, influenced by different surrounding lithologies. Similar to type II events, earthquakes represent the likeliest trigger for these event layers (Wilhelm et al., 2012). This is further supported by the fact that according to the SG06 age model, EL-91 occurred around AD 1660 and is therefore most likely related to the AD 1662 earthquake.

4.2. Facies change at EL-3107 (38,213 $SG06_{2012}$ yr BP)

As stated earlier, the change from a clastic rich to a clastic poor facies occurs very suddenly and is marked by the event layer EL-3107 (type II, Fig. 4). Therefore, it appears likely that event sedimentation and facies change are related.

The high content of clastic material below event layer EL-3107 suggests that Lake Mikata did not act as a filter for the detrital material. Probably the Hasu River did not discharge into Lake Mikata at the time, but into Lake Suga, which has a much wider and sloping connection to Lake Suigetsu and therefore a lesser filtering effect on the detrital material. The East coast of Lake Suga shows a possible inflow point for the Hasu River, characterised by a rather flat morphology (Fig. 1). If this were indeed the case, a mechanism is needed that shifted the Hasu River estuary from Lake Suga to Lake Mikata, 'turning the filter on'. An earthquake blocking/moving the old riverbed, analogous to the AD 1662 displacement of the lake system outlet (see Section 1.1), is the most likely explanation. It would not only explain the very sudden facies change, but also EL-3107 marking the transition, with the event layer having been triggered by the earthquake (in concordance with the interpretation of type II event layers).

An effect on the flood layer frequency by this change in the hydrology is not evident. However, since this change is close to the base of the analysed interval (Fig. 6), the data available from below the event layer are limited.

4.3. Comparison with earlier findings from Lake Suigetsu

Compared to the study of Katsuta et al. (2007), we have identified a considerably higher number of event layers (about 3 times as many in the common interval of the two studies), which we relate to a higher sensitivity of the multi-proxy identification approach applied here. Furthermore, Katsuta et al. (2007) assumed that turbidites are generally the results of earthquakes and clay layers the result of floods. Our data suggest that clay layers represent the clay cap of (type I) turbidites and represent cases in which the coarsest material did not reach the drilling location (i.e. the I-A sub-layer did not form at the drilling location). Hence, we propose that most turbidites (type I) relate to floods and only a minor number to earthquakes (type II). Event layer types II and III have not been described before and are reported here for the first time, both likely to be related to earthquakes.

4.4. Flood layer frequency

Detrital layer frequency and flood frequency are related but not identical and, unless there is other evidence, it must be assumed that not all floods are represented by detrital flood layers in the sediment record (Kämpf et al., 2012). Thresholds to when a flood produces an associated layer depend on variables such as flow speed, entry point into the lake, morphology of the lake site and weathering rates (Sturm and Matter, 1978; Czymzik et al., 2010; Gilli et al., 2013). Earthquakes are another process of physical weathering leading to additional sediment delivery in tectonically active regions like Japan. Hovius et al. (2011) and Howarth et al. (2012) showed that a strong earthquake can significantly increase the amount of easily erodible material in a catchment and that the material can be taken up by surface runoff for several years after the actual earthquake, thereby increasing the likelihood of the formation of a flood layer after a precipitation event in that time. Another influence on the sedimentary flood record is the flood layer geometry. Flood layers usually do not form homogeneously over the lake floor, so that the coring position relative to the entry point of the floods influences the number of layers found in the core. In distal positions flood layers may not be present when the energy of the turbidity current was rather low (Kämpf et al., 2012), in proximal positions older flood layers can be eroded by later turbidity currents (Sturm and Matter, 1978).

The flood layer frequency (i.e. event layer type I frequency) values reported here are smaller than in comparable studies from other sites (e.g. Czymzik et al., 2010; Swierczynski et al., 2012) by a factor of 5–15. One possible reason for this fact is that this study only includes flood layers thicker than 1 mm in order to record primarily the strong flood events. Even though flood layer thickness and flood magnitude are not directly proportional to one another, there is a general trend that larger floods produce thicker detrital layers (Kämpf et al., 2012). This relationship might be even more pronounced for the Suigetsu sediments due to the specific hydrologic situation. Lake Mikata, linked to Lake Suigetsu in the South, acts as an effective sediment trap for suspended material transported by the Hasu River, which is the main discharge channel in the region and which discharges into Lake Mikata. This interpretation is supported by thickness measurements of the layer EL-1433.5 for which thin sections from two sediment cores (SG06 and SG93) are available. The layer is 95% thinner in the more southern SG93 core which is located proximal to the connection to Lake Mikata and thus the thickness difference indicates that sediment delivery occurred from other directions. Only flood discharges that entered Lake Suigetsu via Lake Suga, which floods can enter at its Eastern shore (Fig. 1), or through linear runoff and erosion events from the local slopes alongside the Suigetsu shoreline could have triggered deposition of detrital flood layers in Lake Suigetsu. The connection between Lake Suga to the East and Lake Suigetsu is much wider and without a distinct threshold resulting in a weaker filtering effect and thereby enabling enhanced sediment transport into Lake Suigetsu and the formation of thick event layers.

As stated earlier, the flood layer frequency (Fig. 6) shows a high variability and the boundaries of two flood layer zones coincide with major climatic changes: FLZ2 occurred at about the same time as H1 and FLZ3 coincides with the glacial sea level lowstand (Lambeck et al., 2002). The onset of FLZ3 also correlates with the onset of colder and drier climate conditions in central Japan, indicated by a decrease in *Cryptomeria japonica* and an increase in *Pinus*, *Tsuga* and *Picea* trees in the Lake Biwa pollen assemblage (Hayashi et al., 2010) (Fig. 6). Lake Biwa pollen data are used here for comparison since pollen data from Lake Suigetsu are not yet finalised for the analysed section. Lake Biwa is located about 20 km Southeast of Lake Suigetsu and is thus expected to reflect the same regional climate signal. The pollen record of Lake Biwa also shows relatively high values of upland herb taxa during FLZ3 and FLZ 2, which suggest moderately open or discontinuous forests (Hayashi

et al., 2010). However, an influence on the erosion rates and subsequently the flood layer frequency is not apparent since the flood layer frequency decreases in FLZ2 while values of upland herb taxa remain high (Hayashi et al., 2010). Furthermore, the strong 2000 yr cyclicity in the flood layer frequency observed in FLZ3 is not present in the pollen data. We also exclude an increase in heavy precipitation events related to the monsoon front as a possible explanation for the high flood layer frequency in FLZ3 since at that time the front was weaker and most likely located further to the South, which caused the colder and drier climatic conditions in Japan. An increase in snowfall and subsequently in the magnitude of snow melts can be ruled out too since at the time the warm Tsushima current did not enter the Sea of Japan due to lower eustatic sea levels (Ono et al., 2005). Therefore, during the winter monsoon season less moisture was taken up and precipitation is likely to have been decreased. This leaves an increase in the summer typhoon frequency in the region as the most likely explanation for the increase in flood layers. This interpretation is in line with coupled ocean–atmosphere model simulations for the LGM, which have revealed an increased potential for tropical cyclone genesis in the central and western North Pacific, despite the generally colder conditions (Korty et al., 2012). An increase in typhoons does not contradict drier climate conditions (Hayashi et al., 2010) or generally reduced erosion rates in Japan (Oguchi et al., 2001, and references therein), since the flood layer record only shows relatively infrequent, extreme events.

The apparent cyclicity of $T \approx 2000$ yr during FLZ3 could be related to solar variation, namely the Hallstatt Cycle. Alternatively, it could also be indicative of an influence of the El Niño Southern Oscillation (ENSO). Today, during central Pacific El Niño years typhoons are more likely to make landfall over Japan (Woodruff et al., 2009; Zhang et al., 2012) and Moy et al. (2002) showed that ENSO exhibited a ≈2000 yr cyclicity over the Holocene. It is quite possible that a similar mode was also operating during FLZ3.

The boundary of the subdivision of FLZ3 coincides with H2, after which $\delta^{18}O$ values in the Hulu Cave (Eastern China) speleothems stabilised (Wang et al., 2001). Even though H2 itself did not leave an imprint on the flood layer record, the climatic change following led to a decrease in the flood layer frequency. Possibly the stabilisation of the monsoon system reduced the typhoons affecting central Japan.

While no significant changes in the flood layer frequency can be observed contemporaneous with H2 and H3, the frequency is strongly reduced during H1, reaching the lowest overall values down to 0 per 1000 yr. Also, the Hulu Cave $\delta^{18}O$ speleothem record reaches its absolute minimum in the last 40 ka in this time frame (Fig. 6). Apparently, the further decreased temperatures greatly reduced the number of typhoons affecting central Japan, leaving no persistent mechanism to cause major flood events.

The following zone FLZ1 is characterised by the three maxima in the flood layer frequency, separated by minima relating to the LGIT stadial and the middle Holocene. This pattern is also mainly responsible for the 5000 yr cyclicity evident in the spectral analysis (Fig. 7). However, this might be a pseudo-cyclicity with the three maxima having independent causes. In particular, the earliest maximum is set apart from the other two. The sudden increase in flood layers coincides precisely with the onset of the LGIT, suggesting some relationship with the sudden warming. Alternatively, the maximum could be related to an increase in erosion rates after an earthquake (Hovius et al., 2011; Howarth et al., 2012), which is indicated by a type III event layer (EL-1731.8) marking the boundary between the Glacial and the LGIT. Furthermore, if the shape in the frequency curve, a sudden increase followed by a slightly slower decrease, is representative of enhanced erosion following earthquakes, then the last peak in FLZ3 at 19,200 $SG06_{2012}$ yr BP might also relate to an earthquake, although there is no earthquake related layer (type II or III) at the base of this maximum. The low number of earthquake related layers (7) over the last 40 ka in such a tectonically active area clearly shows that not every earthquake produces an associated event layer. Therefore, the absence of an earthquake-related layer does not exclude the occurrence of an earthquake.

The early Holocene is characterised by increased flood frequency values compared to the LGIT, which persist until ≈8000 $SG06_{2012}$ yr BP. The remainder of the Holocene shows generally lower values than during the early Holocene, with a weak minimum in the middle Holocene between ≈8000 and ≈5000 $SG06_{2012}$ yr BP. The trend towards lower values in the middle and late Holocene can be attributed to a decrease in summer insolation (associated with an increase in winter insolation), weakening the monsoon system (Zhao et al., 2009). The minimum in the mid Holocene could be the result of lower solar activity at the time (Solanki et al., 2004; Steinhilber et al., 2009). The reduction in the flood layer frequency at 8000 $SG06_{2012}$ yr BP is also interesting with respect to winter precipitation, since the Tsushima current entered the Sea of Japan again at the time (Takei et al., 2002). But rather than an increase in flood layers due to additional snow melt-triggered layers, the flood layer frequency declines, which suggests that snow melts had only a minor impact on the flood layer frequency.

A solar influence on the flood layer frequency is not only suggested by the minimum in the middle Holocene, but also by the spectral analysis, with the 2000 yr cycle possibly relating to the Hallstatt Cycle (see above) and the 220 yr cycle probably reflecting the de Vries (Suess) Cycle.

Lastly, the pattern of FLZ5 and FLZ4 is difficult to interpret since the character of FLZ5 beyond 40 ka BP is unknown. Furthermore, the pattern is not mirrored in other key records from the region, which might indicate a local change. This illustrates that floods are short-term meteorological events and that a straightforward relationship with climate patterns is not a matter of course.

5. Conclusions

The flood layer frequency in Lake Suigetsu shows a complex progression. Prior to about 30 ka BP it appears to reflect local changes, later it is clearly influenced by northern hemispheric climate patterns. But even after 30 ka BP non-climatic mechanisms influenced the flood layer record. Earthquakes appear to have had an impact on the flood frequency on two occasions, increasing the amount of erodible material and subsequently increasing the number of flood layers formed. This means that flood layer records are not straightforward proxies for climate change *per se* and that the influence of processes in the catchment must be carefully ascertained. Despite these additional influences, clear climate driven changes in the flood layer frequency are evident. In this respect it is most surprising that between 30 and 18.5 $SG06_{2012}$ ka BP the flood layer frequency reaches its highest mean and absolute values, although this was an episode of cold and dry climate in Japan. Other cold episodes such as H1 and the LGIT stadial show clearly reduced flood layer frequency values, in the case of H1 even the lowest overall values. The warm and wet Holocene shows intermediate values between the two extremes. These differences between wet and dry episodes show that short term extreme precipitation was decoupled from the centennial to millennial average precipitation. Furthermore, the large scale changes in the flood layer frequency appear to have been modulated by solar activity. Changes in typhoon genesis and/or typhoon tracks appear to be the likeliest explanation for the variability of the flood layer frequency during the Glacial. In the Holocene it is

unclear whether extreme precipitation events were related to typhoons or rather to the monsoon front. But it could be shown that snow melts had only a minor impact on the record.

In summary, the data illustrate that the microfacies analysis of event layers in lacustrine sediments provides highly valuable proxy data for improving our understanding of (palaeo-) environmental mechanisms in the East Asian realm. In the future, detailed comparison with high-resolution pollen (and other proxy) data directly from Lake Suigetsu offers the potential to gain a further improved understanding of the site specific climatic and hydrological changes and to separate their individual impacts on the flood layer record.

Acknowledgements

We thank the German Research Foundation (DFG grants TA-540/3-1, BR 2208/7-1), the UK Natural Environment Research Council (NERC grants NE/D000289/1, NE/F003048/1, SM/1219.0407/001), the KAKENHI project of Japan (grant 211001002) and INTIMATE EU cost for funding. Furthermore, we thank Prof. K. Takemura for providing map material of the Lake Suigetsu region and Dr. R. Hayashi for providing the raw Lake Biwa pollen data. We also thank the two anonymous reviewers for their suggestions, which helped us to improve the manuscript. The data presented here are available online at http://dx.doi.org/10.1594/PANGAEA.821829.

References

Arnaud, F., Lignier, V., Revel, M., Desmet, M., Beck, C., Pourchet, M., Charlet, F., Trentesaux, A., Tribovillard, N., 2002. Flood and earthquake disturbance of ^{210}Pb geochronology (Lake Anterne, NW Alps). Terra Nova 14, 225–232.

Beck, C., 2009. Late Quaternary lacustrine paleo-seismic archives in north-western Alps: examples of earthquake-origin assessment of sedimentary disturbances. Earth-Sci. Rev. 96, 327–344.

Brauer, A., Casanova, J., 2001. Chronology and depositional processes of the laminated sediment record from Lac d'Annecy, French Alps. J. Paleolimnol. 25, 163–177.

Brauer, A., Mangili, C., Moscariello, A., Witt, A., 2008. Palaeoclimatic implications from micro-facies data of a 5900 varve time series from the Pànico interglacial sediment record, Southern Alps. Palaeogeogr. Palaeoclimatol. Palaeoecol. 259, 121–135.

Bronk Ramsey, C., Staff, R.A., Bryant, C.L., Brock, F., Kitagawa, H., van der Plicht, J., Schlolaut, G., Marshall, M.H., Brauer, A., Lamb, H.F., Payne, R.L., Tarasov, P.E., Haraguchi, T., Gotanda, K., Yonenobu, H., Yokoyama, Y., Tada, R., Nakagawa, T., 2012. A complete terrestrial radiocarbon record for 11.2 to 52.8 kyr B.P. Science 338, 370–374.

Cockburn, J.M.H., Lamoreux, S.F., 2007. Century-scale variability in late-summer rainfall events recorded over seven centuries in subannually laminated lacustrine sediments, White Pass, British Columbia. Quat. Res. 67, 193–203.

Czymzik, M., Brauer, A., Dulski, P., Plessen, B., Naumann, R., von Grafenstein, U., Scheffler, R., 2013. Orbital and solar forcing of shifts in Mid- to Late Holocene flood intensity from varved sediments of pre-alpine Lake Ammersee (southern Germany). Quat. Sci. Rev. 61, 96–110.

Czymzik, M., Dulski, P., Plessen, B., von Grafenstein, U., Naumann, R., Brauer, A., 2010. A 450 year record of spring-summer flood layers in annually laminated sediments from Lake Ammersee (southern Germany). Water Resour. Res. 46.

Fukutome, S., Frei, C., Schär, C., 2003. Interannual covariance between Japan Summer Precipitation and Western North Pacific SST. J. Meteorol. Soc. Jpn. 81, 1435–1456.

Gilli, A., Anselmetti, F.S., Glur, L., Wirth, S.B., 2013. Lake sediments as archives of recurrence rates and intensities of past flood events. In: Schneuwly-Bollschweiler, M., Stoffel, M., Rudolf-Miklau, F. (Eds.), Dating Torrential Processes on Fans and Cones – Methods and Their Application for Hazard and Risk Assessment, Advances in Global Change Research, vol. 47, pp. 225–242.

Grossman, M.J., 2001. Large floods and climatic change during the Holocene on the Ara River, Central Japan. Geomorphology 39, 21–37.

Hayashi, R., Takahara, H., Hayashida, A., Takemura, K., 2010. Millennial-scale vegetation changes during the last 40,000 yr based on a pollen record from Lake Biwa, Japan. Quat. Res. 74, 91–99.

Hoffmann, D.L., Beck, J.W., Richards, D.A., Smart, P.L., Singarayer, J.S., Ketchmark, T., Hawkesworth, C.J., 2010. Towards radiocarbon calibration beyond 28 ka using speleothems from the Bahamas. Earth Planet. Sci. Lett. 289, 1–10.

Hovius, N., Meunier, P., Lin, C.W., Chen, H., Chen, Y.G., Dadson, S., Horng, M.J., Lines, M., 2011. Prolonged seismically induced erosion and the mass balance of a large earthquake. Earth Planet. Sci. Lett. 304, 347–355.

Howarth, J.D., Fitzsimons, S.J., Norris, R.J., Jacobsen, G.E., 2012. Lake sediments record cycles of sediment flux driven by large earthquakes on the Alpine fault, New Zealand. Geology 40, 1091–1094.

Jessen, K., 1935. Archaelogical dating in the history of North Jutland's vegetation. Acta Archaeol. 5, 185–214.

Kämpf, L., Brauer, A., Dulski, P., Lami, A., Marchetto, A., Gerli, S., Ambrosetti, W., Guilizzoni, P., 2012. Detrital layers marking flood events in recent sediments of Lago Maggiore (N. Italy) and their comparison with instrumental data. Freshw. Biol. 57, 2076–2090.

Katsuta, N., Takano, M., Kawakami, S.-I., Togami, S., Fukusawa, H., Kumazawa, M., Yasuda, Y., 2006. Climate system transition from glacial to interglacial state around the beginning of the last termination: evidence from a centennial-to millennial-scale climate rhythm. Geochem. Geophys. Geosyst. 7.

Katsuta, N., Takano, M., Kawakami, S.-I., Togami, S., Fukusawa, H., Kumazawa, M., Yasuda, Y., 2007. Advanced micro-XRF method to separate sedimentary rhythms and event layers in sediments: its application to lacustrine sediment from Lake Suigetsu, Japan. J. Paleolimnol. 37, 259–271.

Kawakami, S.-I., Fukusawa, H., Kanaori, Y., 1996. A new opportunity to detect paleoearthquake events dating back to the past 10 millennia: a record from lacustrine sediment. Eng. Geol. 43, 177–188.

Kitagawa, H., Fukuzawa, H., Nakamura, T., Okumura, M., Takemura, K., Hayashida, A., Yasuda, Y., 1995. AMS ^{14}C dating of varved sediments from Lake Suigetsu, Central Japan and atmospheric ^{14}C change during the Late Pleistocene. Radiocarbon 37, 371–378.

Kitagawa, H., van der Plicht, J., 2000. Atmospheric radiocarbon calibration beyond 11,900 cal BP from Lake Suigetsu laminated sediments. Radiocarbon 42, 369–380.

Kondo, R., Nakagawa, A., Mochizuki, L., Osawa, K., Fujioka, Y., Butani, J., 2009. Dominant bacterioplankton populations in the meromictic Lake Suigetsu as determined by denaturing gradient gel electrophoresis of 16S rRNA gene fragments. Limnology 10, 63–69.

Korty, R.L., Camargo, S.J., Galewsky, J., 2012. Tropical cyclone genesis factors in simulations of the Last Glacial Maximum. J. Clim. 25, 4348–4365.

Lambeck, K., Yokoyama, Y., Purcell, T., 2002. Into and out of the Last Glacial Maximum: sea-level change during Oxygen Isotope Stages 3 and 2. Quat. Sci. Rev. 21, 343–360.

Lauterbach, S., Chapron, E., Brauer, A., Hüls, M., Gilli, A., Arnaud, F., Piccin, A., Nomade, J., Desmet, M., von Grafenstein, U., Participants, DecLakes, 2012. A sedimentary record of Holocene surface runoff events and earthquake activity from Lake Iseo (Southern Alps, Italy). Holocene 22, 749–760.

Mangerud, J., Andersen, S.T., Berglund, B.E., Donner, J.J., 1974. Quaternary stratigraphy of Norden, a proposal for terminology and classification. Boreas 3, 109–126.

Mangili, C., Brauer, A., Moscariello, A., Naumann, R., 2005. Microfacies of detrital event layers deposited in Quaternary varved lake sediments of the Pànico-Sèllere Basin (northern Italy). Sedimentology 52, 927–943.

Marshall, M., Schlolaut, G., Brauer, A., Nakagawa, T., Staff, R.A., Bronk Ramsey, C., Lamb, H., Gotanda, K., Haraguchi, T., Yokoyama, Y., Yonenobu, H., Tada, R., SG06 project members, 2012. A novel approach to varve counting using μXRF and X-radiography in combination with thin-section microscopy, applied to the Late Glacial chronology from Lake Suigetsu, Japan. Quat. Geochronol. 13, 70–80.

Masuzawa, T., Kitano, Y., 1982. Sulfate reduction and sulfur fixation in sediment of a historically meromictic lake, Lake Suigetsu, Japan. J. Oceanogr. 38, 21–27.

Moreno, A., Valero-Garcés, B.L., González-Sampériz, P., Rico, M., 2008. Flood response to rainfall variability during the last 2000 years inferred from the Taravilla Lake record (Central Iberian Range, Spain). J. Paleolimnol. 40, 943–961.

Moy, C.M., Seltzer, G.O., Rodbell, D.T., Anderson, D.M., 2002. Variability of El Niño/Southern Oscillation activity at millennial timescales during the Holocene epoch. Nature 420, 162–165.

Mulder, T., Alexander, J., 2001. The physical character of subaqueous sedimentary density flows and their deposits. Sedimentology 48, 269–299.

Nakagawa, T., Gotanda, K., Haraguchi, T., Danhara, T., Yonenobu, H., Brauer, A., Yokoyama, Y., Tada, R., Takemura, K., Staff, R.A., Payne, R., Bronk Ramsey, C., Bryant, C., Brock, F., Schlolaut, G., Marshall, M., Tarasov, P., Lamb, H., 2012. SG06, a fully continuous and varved sediment core from Lake Suigetsu, Japan: stratigraphy and potential for improving the radiocarbon calibration model and understanding of late Quaternary climate changes. Quat. Sci. Rev. 36, 164–176.

Nakagawa, T., Kitagawa, H., Yasuda, Y., Tarasov, P.E., Gotanda, K., Sawai, Y., 2005. Pollen/event stratigraphy of the varved sediment of Lake Suigetsu, central Japan from 15,701 to 10,217 SG vyr BP (Suigetsu varve years before present): description, interpretation, and correlation with other regions. Quat. Sci. Rev. 24, 1691–1701.

Nakagawa, T., Tarasov, P.E., Kitagawa, H., Yasuda, Y., Gotanda, K., 2006. Seasonally specific responses of the East Asian monsoon to deglacial climate changes. Geology 34, 521–524.

Oguchi, T., Saito, K., Kadomura, H., Grossman, M., 2001. Fluvial geomorphology and paleohydrology in Japan. Geomorphology 39, 3–19.

Ono, Y., Aoki, T., Hasegawa, H., Dali, L., 2005. Mountain glaciation in Japan and Taiwan at the global Last Glacial Maximum. Quat. Int. 138–139, 79–92.

Reimer, P.J., Baillie, M.G.L., Bard, E., Bayliss, A., Beck, J.W., Blackwell, P.G., Bronk Ramsey, C., Buck, C.E., Burr, G.S., Edwards, R.L., Friedrich, M., Grootes, P.M.,

Guilderson, T.P., Hajdas, I., Heaton, T.J., Hogg, A.J., Hughen, K.A., Kaiser, K.F., Kromer, B., McCormac, F.G., Manning, S.W., Reimer, R.W., Richards, D.A., Southon, J.R., Talamo, S., Turney, C.S.M., van der Plicht, J., Weyhenmeyer, C.E., 2009. IntCal09 and Marine09 radiocarbon age calibration curves, 0–50,000 years cal BP. Radiocarbon 51, 1111–1150.

Schlolaut, G., Marshall, M.H., Brauer, A., Nakagawa, T., Lamb, H.F., Staff, R.A., Bronk Ramsey, C., Bryant, C.L., Brock, F., Kossler, A., Tarasov, P.E., Yokoyama, Y., Tada, R., Haraguchi, T., Suigetsu 2006 project members, 2012. An automated method for varve interpolation and its application to the Late Glacial chronology from Lake Suigetsu, Japan. Quat. Geochronol. 13, 52–69.

Schulz, M., Mudelsee, M., 2002. REDFIT: estimating red-noise spectra directly from unevenly spaced paleoclimatic time series. Comput. Geosci. 28, 421–426.

Schulz, M., Stattegger, K., 1997. SPECTRUM: spectral analysis of unevenly spaced paleoclimatic time series. Comput. Geosci. 23, 929–945.

Smith, V.C., Staff, R.A., Blockley, S.P.E., Bronk Ramsey, C., Nakagawa, T., Mark, D.F., Takemura, K., Danhara, T., Suigetsu 2006 Project Members, 2013. Identification and correlation of visible tephras in the Lake Suigetsu SG06 sedimentary archive, Japan: chronostratigraphic markers for synchronising of east Asian/west Pacific palaeoclimatic records across the last 150 ka. Quat. Sci. Rev. 67, 121–137.

Solanki, S.K., Usoskin, I.G., Kromer, B., Schüssler, M., Beer, J., 2004. Unusual activity of the Sun during recent decades compared to the previous 11,000 years. Nature 431, 1084–1087.

Southon, J., Noronha, A.L., Cheng, H., Edwards, R.L., Wang, Y., 2012. A high-resolution record of atmospheric ^{14}C based on Hulu Cave speleothem H82. Quat. Sci. Rev. 33, 32–41.

Staff, R.A., Bronk Ramsey, C., Bryant, C.L., Brock, F., Payne, R.L., Schlolaut, G., Marshall, M.H., Brauer, A., Lamb, H.F., Tarasov, P., Yokoyama, Y., Haraguchi, T., Gotanda, K., Yonenobuk, H., Nakagawa, T., Suigetsu 2006 project members, 2011. New ^{14}C determinations from Lake Suigetsu, Japan: 12,000 to 0 cal BP. Radiocarbon 53, 511–528.

Staff, R.A., Nakagawa, T., Schlolaut, G., Marshall, M.H., Brauer, A., Lamb, H., Bronk Ramsey, C., Bryant, C.L., Brock, F., Kitagawa, H., van der Plicht, J., Payne, R.L., Smith, V.C., Mark, D.F., MacLeod, A., Blockley, S.P.E., Schwenninger, J.L., Tarasov, P., Haraguchi, T., Gotanda, K., Yonenobu, H., Yokoyama, Y., Suigetsu 2006 project members, 2013a. The multiple chronological techniques applied to the Lake Suigetsu (SG06) Sediment Core. Boreas 42, 259–266.

Staff, R.A., Schlolaut, G., Bronk Ramsey, C., Brock, F., Bryant, C.L., Kitagawa, H., van der Plicht, J., Marshall, M.H., Brauer, A., Lamb, H., Payne, R.L., Tarasov, P., Haraguchi, T., Gotanda, K., Yonenobu, H., Yokoyama, Y., Nakagawa, T., Suigetsu 2006 project members, 2013b. Integration of the old and new Lake Suigetsu (Japan) terrestrial radiocarbon calibration data sets. Radiocarbon 55 (in press).

Stanford, J.D., Rohling, E.J., Bacon, S., Roberts, A.P., Grousset, F., Bolshaw, M., 2011. A new concept for the paleoceanographic evolution of Heinrich event 1 in the North Atlantic. Quat. Sci. Rev. 30, 1047–1066.

Steinhilber, F., Beer, J., Fröhlich, C., 2009. Total solar irradiance during the Holocene. Geophys. Res. Lett. 36.

Sturm, M., Matter, A., 1978. Turbidites and varves in Lake Brienz (Switzerland): deposition of Clastic Detritus by Density Currents. Spec. Publ. Int. Assoc. Sedimentol. 2, 147–168.

Swierczynski, T., Brauer, A., Lauterbach, S., Martín-Puertas, C., Dulski, P., von Grafenstein, U., Rohr, C., 2012. A 1600 yr seasonally resolved record of decadal-scale flood variability from the Austrian Pre-Alps. Geology 40, 1047–1050.

Takano, Y., Tachibana, Y., Iwamoto, K., 2008. Influences of large-scale atmospheric circulation and local sea surface temperature on convective activity over the sea of Japan in December. Sola 4, 113–116.

Takei, T., Minoura, K., Tsukawaki, S., Nakamura, T., 2002. Intrusion of a branch of the Oyashio Current into the Japan Sea during the Holocene. Paleoceanography 17, 11-1–11–10.

Torrence, C., Compo, G.P., 1998. A practical guide to wavelet analysis. Bull. Am. Meteorol. Soc. 79, 61–78.

Vasskog, K., Nesje, A., Støren, E.N., Waldmann, N., Chapron, E., Ariztegui, D., 2011. A Holocene record of snow-avalanche and flood activity reconstructed from a lacustrine sedimentary sequence in Oldevatnet, western Norway. Holocene 21, 597–614.

Wang, Y.J., Cheng, H., Edwards, R.L., An, Z.S., Wu, J.Y., Shen, C.C., Dorale, J.A., 2001. A high-resolution absolute-dated late Pleistocene monsoon record from Hulu Cave, China. Science 294, 2345–2348.

Wilhelm, B., Arnaud, F., Enters, D., Allignol, F., Legaz, A., Magand, O., Revillon, S., Ciguet-Covex, C., Malet, E., 2012. Does global warming favour the occurrence of extreme floods in European Alps? First evidence from a NW Alps proglacial lake sediment record. Clim. Change 113, 563–581.

Woodruff, J.D., Donnelly, J.P., Okusu, A., 2009. Exploring typhoon variability over the mid- to -late Holocene: evidence of extreme coastal flooding from Kamikoshiki, Japan. Quat. Sci. Rev. 28, 1774–1785.

Yarincik, K.M., Murray, R.W., 2000. Climatically sensitive eolian and hemipelagic deposition in the Cariaco Basin, Venezuela, over the past 578,000 years: results from Al/Ti and K/Al. Paleoceanography 15, 210–228.

Yuan, D., Cheng, H., Edwards, R.L., Dykoski, C.A., Kelly, M.J., Zhang, M., Qing, J., Lin, Y., Wang, Y., Wu, J., Dorale, J.A., An, Z., Cai, Y., 2004. Timing, duration, and transitions of the Last Interglacial Asian Monsoon. Science 304, 575–578.

Zhang, W., Graf, H.-F., Leung, Y., Herzog, M., 2012. Different El Niño types and tropical cyclone landfall in East Asia. J. Clim. 25, 6510–6523.

Zhao, Y., Yu, Z., Chen, F., 2009. Spatial and temporal patterns of Holocene vegetation and climate changes in arid and semi-arid China. Quat. Int. 194, 6–18.